Desalination and Water Treatment
www.deswater.com

doi: 10.5004/dwt.2018.23111

136 (2018) 306–319
December

Impact of structure and morphology of titanate nanomaterials on Pb^{2+} adsorption in aqueous solution

Huiping Peng[a,†], Gongduan Fan[a,*,†], Xiaomei Zheng[a], Jing Luo[b], Jinjin Zhou[a]

[a]*College of Civil Engineering, Fuzhou University, 350116 Fujian, China; emails: fgdfz@fzu.edu.cn (G. Fan), Tel. +0086 591 22865361; Fax: 0086 591 22865355, emails: n160527036@fzu.edu.cn (H. Peng), n160520053@fzu.edu.cn (X. Zheng), n170520055@fzu.edu.cn (J. Zhou)*
[b]*Fujian Minke Environmental Technology Development Co., Ltd, Fuzhou, 350002 Fujian, China, Tel. 0086 591 22865361; Fax: 0086 591 22865355; email: 727919985@qq.com*

Received 19 March 2018; Accepted 11 September 2018

ABSTRACT

The impacts of structure and morphology of titanate nanomaterials (TNs) synthesized by simple hydrothermal method on the lead (Pb^{2+}) adsorption in aqueous solutions were systematically evaluated and clarified. The physical-chemical properties of the TNs including chemical composition, morphology, surface area, and structure were characterized. The adsorption capacity, kinetics, equilibrium model, and mechanism of as-prepared TNs were investigated. The results showed that the structure and morphology of TNs change with the reaction temperature and reaction time. The flaky structure of TNs was formed at 100°C and 130°C with reaction time of 24 h, or 12–36 h under the temperature of 130°C. Under 150°C and 180°C with 24 h, 48 h, or more with temperature of 130°C, the synthesized structure was linear. The flakes structure of TNs had higher adsorption capacity for Pb^{2+} than linear structure. The adsorption capacity on Pb^{2+} was up to 504.12 mg/g, and the adsorption kinetics for Pb^{2+} followed pseudo-second-order model. The equilibrium data were in accordance with Langmuir model. The adsorption of heavy metals by flaky TNs could be attributed to the interaction of heavy metal ions with hydroxyl groups in TNs. This study has shown that titanate nanosheets could be a potential adsorbent for the removal of Pb^{2+} from aqueous solution.

Keywords: Titanate nanomaterials; Hydrothermal reaction; Morphology; Adsorption kinetics; Lead

1. Introduction

With the development of industry and rapid urbanization, heavy metal pollution become more and more serious and arouse broad attention. The treatment of industrial wastewater is one of the most pressing problems for a lot of heavy metal ions contained, such as Pb^{2+}, Cd^{2+}, Cr^{6+}, Hg^{2+}, and Ni^{2+} [1] . Heavy metals ions even at a relatively low concentration may be highly toxic and carcinogenic due to its persistence and difficult biodegradation in living tissues through food chain [2]. Therefore, heavy metal pollutions must be eliminated to alleviate the harmful effects on human health and aquatic ecosystems. Effective removal of heavy metal ions from the aqueous solutions is important to protect the environment and public health.

Pb^{2+} is one of highly toxic and bio-accumulative pollutants, participating in various conversion processes in water. So far, several methods have been used to remove heavy metals from aqueous solutions, such as chemical precipitation, membrane filtration [3], electrochemistry [4], and adsorption. Thereinto, adsorption is a simple, flexible, cost-effective, and promising method in applications [5,6]. Traditionally, many natural materials and by-products have been used to remove heavy metals from wastewater, such as organosilane functionalized mesoporous silica, zeolites, bentonite, fungal biomass, shells, and sawdust [7–10]. While these materials have some shortages, such as low adsorption capacity, long equilibrium time, and complex regeneration process. Therefore, searching for regenerated adsorbents with higher adsorption capacity is still in great need [11].

* Corresponding author.

† These authors contributed equally to this work.

In recent years, titanate nanomaterials (TNs) hydrothermally prepared by TiO_2 and NaOH are of great interest and have been commonly used in many research fields, including photocatalysis [12,13], solar energy conversion [14,15], lithium ion battery [16,17], and in the removal of toxic pollutants [18,19] from wastewater containing reactive dyestuffs and heavy metal substances [20]. Compared with other adsorbents, the preparation conditions of TNs such as agitated reactors, reaction pressure, and temperatures can be easily satisfied. It is particularly noteworthy that TNs are widely used as heavy metal adsorbents due to their unique physicochemical properties, strong ion exchange performance, large specific surface area and low secondary pollution [21], which are considered promising materials for adsorption application. It is worth noting that TNs were surface charged as the existence of many functional hydroxyl groups, which resulted in the ion-exchange properties [22]. The advantage of some TNs is the collapse of their structure, which occurs during the ion exchange and lead to tight immobilization of targeted cations in the interlayer, thus in irreversible ion exchange [23].

Up to the present, numerous studies have focused on the adsorption behavior of titanate nanotubes (TNTs). TNT has good adsorption capability for Pb^{2+} and Cr^{2+}, and its adsorption capacity can reach up to 520.83 and 238.61 mg/g, respectively [24]. External diffusion is the main control process of Cu^{2+} adsorbed by TNT, and the adsorption kinetics of Cu^{2+} on TNT follows the pseudo-second-order model [25]. In addition, the adsorption mechanism of TNT is mostly cation exchange. At low Pd content, Pd is adsorbed by TNT in a cation-exchange mode. When Pd concentration is above 1.13 mmol/g, the precipitation of a large amount of Pd salt would occur [26]. Although plentiful researches have been made on the adsorption of heavy metals on TNTs, less attention has been paid to Pb^{2+} adsorptions onto other forms of TNs, and the interaction between heavy metals ions and forms of TNs has not been well described.

The property of the adsorbent depends on the preparation process. Different composition and morphology of the prepared material will be obtained under different reaction conditions. Different reaction temperature and synthesis time have a significant impact on the morphology of TNs and the adsorption properties of heavy metals [27–29]. For example, nanofiber was found very effective in adsorbing Cu^{2+} and Pb^{2+} ions with high equilibrium adsorption capacities about 485.44 and 263.15 mg/g, respectively [30,31]. Besides, the chitosan/poly(ethylene oxide) (PEO) nanofibrous membrane having no beads, mesopores, and high specific surface area. Thus, it possesses the maximum adsorption capacity for Cu^{2+}, Zn^{2+}, and Pb^{2+} ions were 120, 117, and 108 mg/g, respectively [32]. TNTs are metastable structures, and every process in the preparation may result in the transformation of their crystalline phases [33]. The mixed crystals of anatase and rutile phases were obtained by hydrothermal treatment at 80°C for 48 h in 1 mol/L HCl solution, while the anatase phase nanorods were obtained at 175°C [34]. Moreover, the hydrothermal reaction time and temperature also have effect on the morphology of the final product of TNs and its adsorption of heavy metal ions. When TiO_2 and 10 M NaOH were reacted at 140°C for 48 h, the resulting TNT would adsorb Pb^{2+} with a capacity of 3.752 mmol/g [35]. However, when the temperature is at 130°C for 3 h, the actual adsorption capacity of Pb^{2+} on TNT could reach 500 mg/g [36]. The maximum adsorption capacity of Pb^{2+} for TNT obtained at 130°C for 72 h could be 520.83 mg/g [24]. It is thus clear evident that the temperature of the hydrothermal reaction and the length of the reaction time have a great influence on the morphology and adsorption properties of TNs.

This study aims to evaluate the effect of reaction temperature and reaction time on the adsorption properties of TNs and the competitive adsorption behaviors of Pb(II), Cd^{2+}, and Ni^{2+} onto TNs prepared by hydrothermal reaction. In addition, this paper systematically studied reaction temperature and reaction time on the morphology, specific surface area, and chemical composition of TNs. Furthermore, we also improved the synthesis conditions to determine the optimal reaction time and reaction temperature.

2. Materials and methods

2.1. Chemical reagents

TiO_2 (titanium dioxide), C_2H_5OH (ethanol), $Pb(NO_3)_2$ (lead^{2+} nitrate), NaOH (sodium hydroxide), and sodium hydroxide (titanium dioxide, 80% anatase, and 20% rutile) were purchased from Sinopharm Group Chemical Reagent Co., Ltd. (Shanghai, China). All chemicals used in this study were of analytical grade, except as a guarantee reagent for $Pb(NO_3)_2$. $Pb(NO_3)_2$ was used to prepare the Pb^{2+} stock solution (1,000 mg/L).

2.2. Preparation of TNs at different reaction temperatures and reaction times

The preparation of TNs mainly referred to the synthesis method of Huang and Li [37], Wang et al. [38], Nadaroglu et al. [39], and Kurniawan [40]. 0.6 g of TiO_2 powder was added to NaOH aqueous solution (10 mol/L, 33 mL), and the mixture was stirred for 24 h at room temperature. After stirring, the mixture was transferred to a 60 mL Teflon container, sealed in a constant temperature at100°C, 130°C, 150°C, and 180°C for 72 h or sealed for 12, 24, 36, 48, 60, and 72 h at 130°C. Cooled to room temperature and washed with deionized water to neutral. Finally, the white precipitate was dried overnight in a dry oven at 70°C, ground, and collected.

2.3. Characterization of TNs

The samples before and after adsorption by Pb^{2+} were all characterized in detail. The sample of the powder to be tested was placed on a glass substrate and compacted with a glass plate. The phase composition of the sample was analyzed by X-ray powder diffraction (XRD) (X'Pert PRO X-ray powder diffraction, PANalytical Co., Ltd, Holland). The radiation source was Co-target $K\alpha$ line, λ = 1.5418 Å, graphite monochromator with a voltage of 35 kV, a current of 35 mA, a scanning step of 0.02°, a scanning speed of 5°/s, a scanning range of 5°–80°, and then a Cu target. The surface morphology, size, and dispensability in the microscopic of the samples were observed by scanning electron microscopy (SEM, S-4800 Scanning Electron Microscope, Japan, accelerated voltage: 5–10 kV). The infrared spectrum of the sample was

measured by Fourier-transform infrared spectroscopy (FT-IR, Nicolet 6700, Thermos Fisher Scientific Co., Ltd, USA), which was previously prepared by KBr pelletizing, with a range of measurement and a separability range of 4,000–400 and 4 cm^{-1}. Brunauer–Emmett–Teller (BET) surface areas were measured by nitrogen adsorption isotherm measurements on a surface area and porosity analyzer (Micromeritics, ASAP2020 HD88, USA) at liquid nitrogen temperature (77 K). Prior to the experiment, the samples were degassed for 10 h at 423 K under vacuum. The concentration of heavy metal ions in the solution was measured by inductively coupled plasma emission spectrometry (ICP-OES Optima 7000, PerkinElmer, USA).

2.4. Adsorption experiment

Adsorption experiments were carried out in tightly closed conical flasks containing 1,000 mL with 1,000 mg/L of Pb^{2+} solutions. Then the suspension was shaken at 200 rpm (20°C) for a certain time. Samples were taken at set time intervals, immediately centrifuged (5,000 rpm) for 5 min and filtered using a 0.45 μm membrane. The supernatant liquid was analyzed by an ICP-OES. The effect of reaction time (0–240 min), adsorption temperature (20°C–60°C), initial pH (1–10), and the dosage of TNs (0–1.0 g/L) were investigated.

2.5. Desorption experiments

The initial concentration C_0 and the equilibrium concentration C_e of Pb^{2+} measured after the TNs dosage were 0.2 or 1.0 g/L and the temperature was 20°C. The pH of the solution was adjusted to 1.0–6.0 using 0.1 M NaOH or HCl. The solution was stirred for 5 h to reach equilibrium again and the desorption equilibrium concentration of Pb^{2+} was measured.

The relevant formula used in the experiment is as follows:

The equilibrium adsorption capacity q_e (mg/g) was calculated by Eq. (1).

$$q_e = \frac{(C_0 - C_e)V}{m} \tag{1}$$

The amount of metal ion adsorbed q_t at time t (min) was calculated by Eq. (2).

$$q_t = \frac{(C_0 - C_t)V}{m} \tag{2}$$

The adsorption rate R (%) is calculated by Eq. (3).

$$R = \frac{C_0 - C_e}{C_0} \times 100 \tag{3}$$

The desorption rate D (%) when desorption to reach equilibrium was calculated by Eq. (4).

$$D = \frac{C_0 - C_e}{C_0 - C_d} \times 100 \tag{4}$$

where C_0 is the initial concentration of heavy metal ions, mg/L; C_e is the equilibrium adsorption concentration of heavy metal ions, mg/L; C_t is the concentration of heavy metal ions at time t, mg/L; m is the titration of TNs; V is the volume of heavy metal ion solution, mL; C_e and C_d (mg/L) are metal equilibrium concentrations of adsorption and desorption, respectively.

2.6. Error analysis

The best fit between the kinetic models was assessed by the squared sum of error (SSE) test which assumes that the model with the lowest SSE values best describes the kinetics of the sorption of the metal ions onto TNs [41]. The following formula is used to calculate SSE:

$$\mathrm{SSE} = \sum_{i=1}^{n} \left(\frac{q_{t,e} - q_{t,m}}{q_{t,e}} \right)^2 \tag{5}$$

where $q_{t,e}$ and $q_{t,m}$ are the experimental adsorption capacities of Pb^{2+} ions in mg/g at time t and the corresponding values obtained from the kinetic models.

The chi-squared (χ^2) tests were adopted to determine the suitability of the isotherm model with respect to the experimental data [42]. The χ^2 equation is as follows:

$$\chi^2 = \sum \frac{(q_e - q_{e,m})^2}{q_{e,m}} \tag{6}$$

where q_e is the experimental equilibrium capacity (mg/g), and $q_{e,m}$ is the equilibrium capacity obtained by calculating from the model (mg/g).

3. Results and discussion

3.1. Characterization of TNs

3.1.1. XRD analysis

3.1.1.1. TNs synthesized at different temperatures The XRD patterns of prepared TNs under the different reaction temperatures are displayed in Fig. 1(a). There were significant differences of the four materials by comparison in the patterns. The prepared TNs-100 was weaker compared with other TNs, demonstrating the material was not fully reacted at 100°C. It could be observed that TNs-130, TNs-150, and TNs-180 had strong diffraction peaks at $2\theta \approx 10°$, and these diffraction peaks could be assigned to Na^+ in TNs (JCPDS file no. 31-1329) [43]. According to the PDF card query, the diffraction peaks could be attributed to the layered structure of TNs [44,45]. It was noteworthy that the main structure of above materials were corresponding to the diffraction peak of anatase TiO_2 (JCPDS file no. 21-1272). In combination with the above analysis, it could be concluded that TNs-130 was a typical TN. Except for the diffraction peaks appear at $2\theta \approx 10°$, 24°, 28° and 48°, there were some hetero-diffraction peaks observed in TNs-150 and TNs-180, which indicated that the increase in temperature had a certain effect on the chemical composition of the material.

3.1.1.2. TNs synthesized at different reaction times The XRD patterns of TNs synthesized at different reaction times are displayed in Fig. 1(b). It illustrated that the spectra of the six materials were basically the same. All peaks in the XRD patterns (Fig. 1(b)) are assigned to the $Na_2Ti_3O_7$ (JCPDS file no. 31-1329) [46]. Based on the previous analysis, the peak at 10° represented the interlayer structure of TNs [47]. Based on the XRD patterns, we can conclude that TNs synthesized at the reaction time varied by 12–72 h were pure monoclinic titanate, and the crystallinity was good. Moreover, it could be confirmed that the chemical composition was $(Na, H)_2Ti_3O_7$ [48].

3.1.2. SEM analysis

3.1.2.1. TNs synthesized at different temperatures The morphology of TNs could be analyzed by SEM. Fig. 2 shows the SEM images of synthesized TNs at different reaction temperatures. From the SEM observation, it could be seen that the TNs prepared at different reaction temperatures exhibits different shapes appearance. TNs-100 and TNs-130 were mainly flaky structure based on the SEM. The morphology of nanosheets was irregular and the thickness was only a few nanometers. The images show that large number of nanosheets were intertwined and superimposed as the shape of flowers, while TNs-150 and TNs-180 were mainly linear structure. The nanowire morphology was more uniform, the length of each nanowire was more than 1 μm and the width

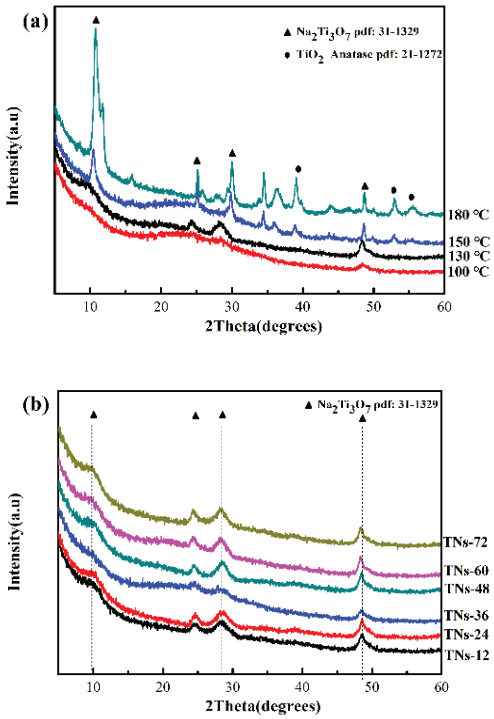

Fig. 1. XRD patterns of TNs: (a) synthesized at different temperatures and (b) synthesized at different reaction times.

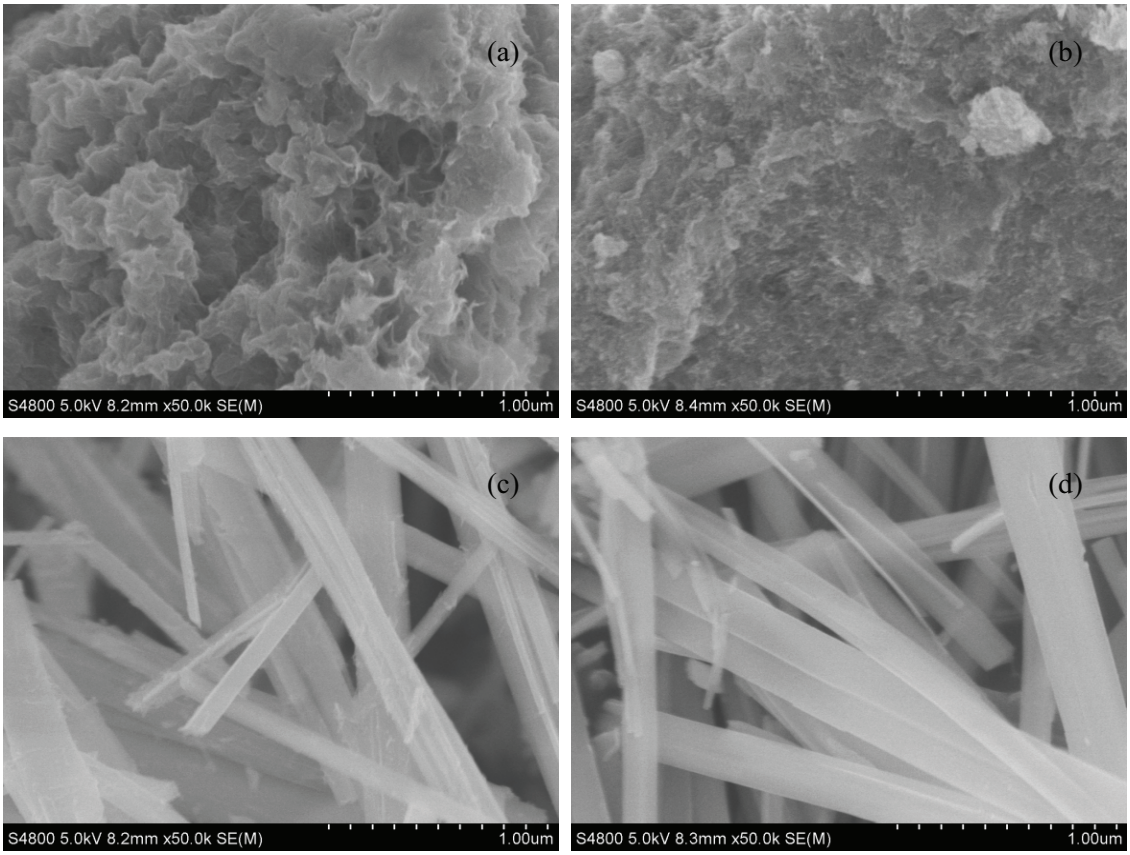

Fig. 2. SEM images of TNs synthesized at different temperatures: (a) TNs-100, (b) TNs-130, (c) TNs-150, and (d) TNs-180.

of the nanowires was tens to 300 nm. From the SEM images, each material was randomly entangled in large number of nanoscale pieces or lines in a disordered state.

3.1.2.2. TNs synthesized at different reaction times To understand the formation mechanism of TNs prepared at different reaction times, the SEM images of the TNs are depicted in Fig. 3. The images showed that the TNs had different morphologies. The morphology of TNs synthesized under 12–36 h were mainly flaky structure. Most of them were only a few nanometers on thickness, and numerous nanoscale pieces were stacked in disordered state into the morphologies of flowers. Although the TNs still had lamellar nanomaterials at 48 h, the linear structure began to appear. That was linear structure with short length which was only a few hundred nanometers for 60 h and 72 h. The SEM showed that each material formed with a great deal of nanosheets or lines in random state and random winding together.

Generally, TNs existed in the form of sheet when the reaction time was in the range of 12–36 h. When the reaction time was 36–72 h, TNs were mainly in the form of tubes. As shown in SEM images, the TNs were only nanoflower structure consisting of flake or linear shape, without the tubular structure. According to the formation mechanism of TiO_2 nanotubes,

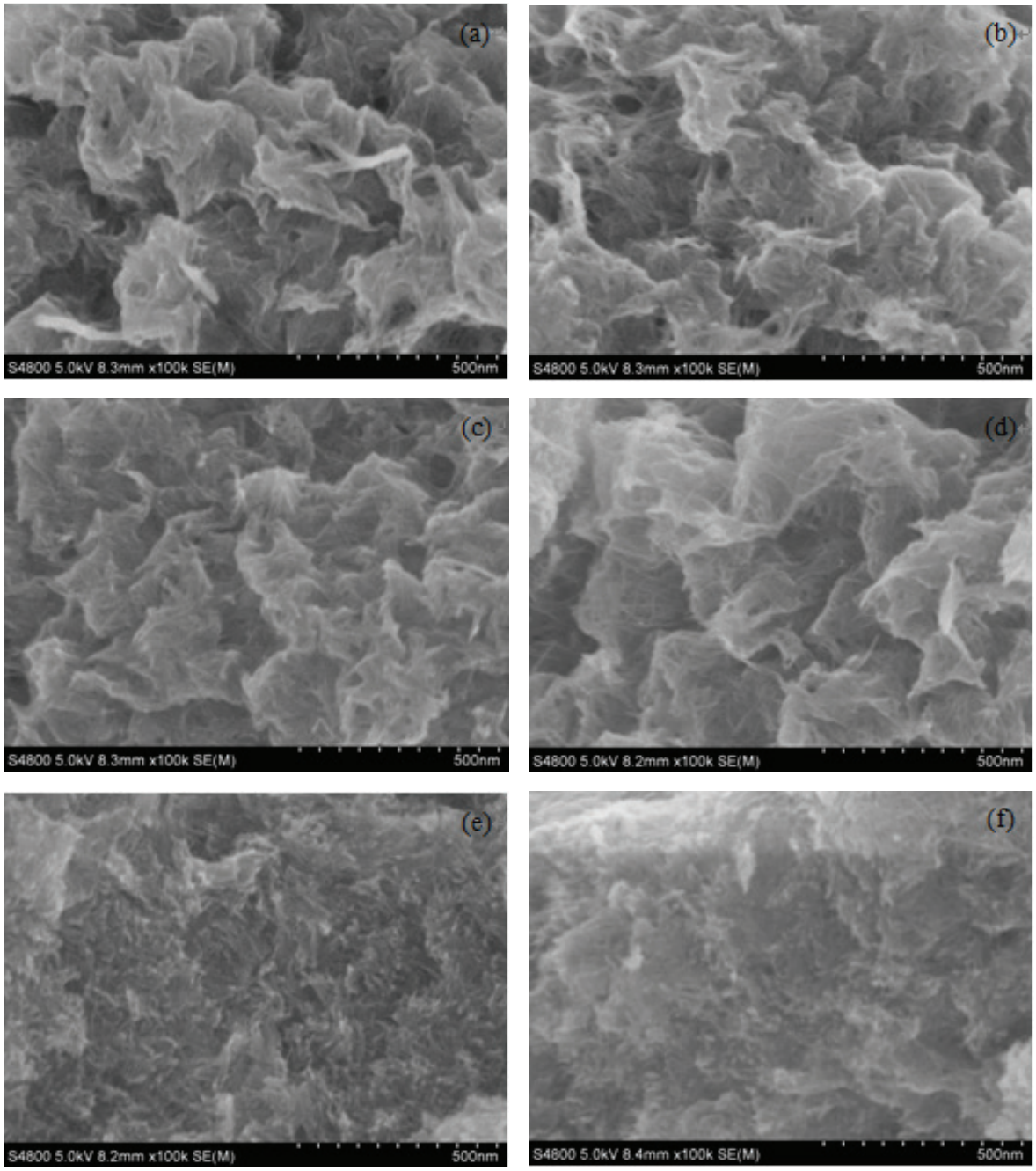

Fig. 3. SEM images of TNs synthesized at different times: (a) TNs-12, (b) TNs-24, (c) TNs-36, (d) TNs-48, (e) TNs-60, and (f) TNs-72.

two-dimensional layered TiO_2 was essential for the formation of tubular. Thus, linear TNs may be an intermediate [49].

3.1.3. FT-IR analysis

The amounts of acid sites and ion-exchange capacities of these samples were determined by FT-IR measurements. Fig. 4(a) shows the FT-IR spectra obtained for the both the flaky TNs-130 before and after adsorption. Before adsorption, the band appeared at 3,344, 1,631, 907, and 486 cm^{-1}, respectively. After adsorption of Pb^{2+} onto flaky TNs-130, the deflection of the stretching vibration of the O–H bond was still large, which was shifted from 3,344 to 3,359 cm^{-1} (offset 14 cm^{-1}). The shift of the O–H band to 3,359 cm^{-1} was due to the interaction of hydroxyl groups with Pb^{2+} in the flaky TNs-130 during the adsorption process.

The FT-IR spectra of flaky TNs-24 adsorbed Pb^{2+} are shown in Fig. 4(b). The main absorption peaks of TNs-24 before absorbed Pb^{2+} appeared at 3,385, 1,631, 907, and 479 cm^{-1}. While for the spectrum of TNs-24 after adsorption of Pb(II), it could be seen that the stretching vibration peak of O–H bond was larger, and it was shifted from 3,385 to 3,352 cm^{-1} (offset of 33 cm^{-1}). As discussed above, the results were also shown that Pb^{2+} interacted with the hydroxyl groups in the flaky TNs during the adsorption process. Therefore, the adsorption mechanism of flaky TNs to Pb^{2+} was mainly due to the ion exchange between Pb^{2+} with H^+/Na^+ in the layer of TNs.

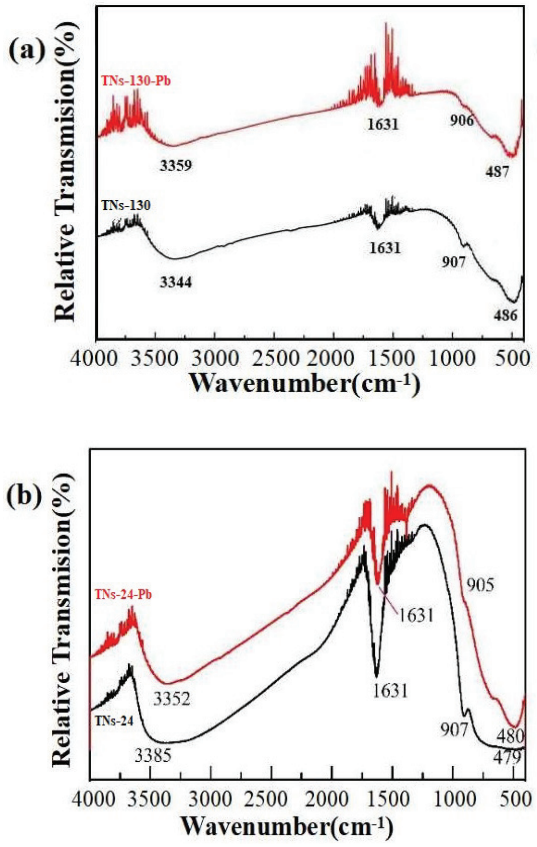

Fig. 4. FT-IR plots of TNs: (a) TNs-130 and (b) TNs-240.

3.1.4. BET analysis

The N_2 adsorption–desorption isotherms of the six TNs are shown in Fig. 5. It can be seen that all six materials are typical type IV isotherms with H3 hysteresis loops [50], indicating the mesoporous properties of the material.

Physical properties of those materials are shown in Table 1. It can be seen from the table that the specific surface areas of the six materials range from 243.05 to 286.20 m^2/g, and the difference is not large. The pore volume ranges from 0.279 to 0.403 cm^3/g. It is reminded here, that the BET surface area of flaky TNs powder is similar to that of linear TNs (Table 1). Therefore, no explicit correlation between adsorption capacity and BET surface areas of the investigated adsorbents can be claimed.

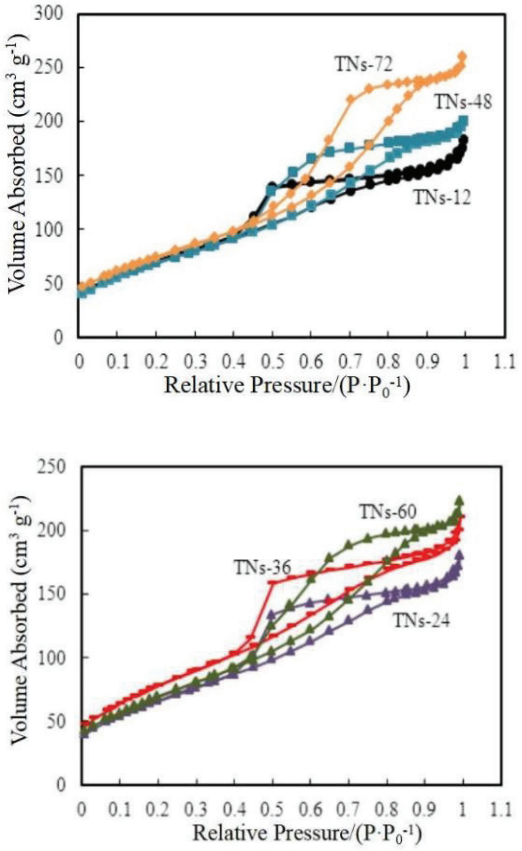

Fig. 5. N_2 adsorption–desorption isotherms of TNs.

Table 1
Basic structure parameters of TNs

	Specific surface area (m^2/g)	Single-point pore volume (cm^3/g)
TNs-12	259.36	0.283
TNs-24	243.05	0.279
TNs-36	286.20	0.325
TNs-48	255.93	0.309
TNs-60	256.10	0.344
TNs-72	274.37	0.403

3.2. Adsorption of Pb^{2+} onto TNs

3.2.1. Removal efficiency of synthesized TNs

The adsorption efficiency of synthesized TNs on the adsorption of Pb^{2+} was conducted to find out the impact of morphology (flaky and linear) to the adsorption capability. The change of adsorption capacity q_e and removal rate R of different initial concentrations of Pb^{2+} on TNs synthesized at different temperatures and different times were shown in Figs. 6 and 7.

As seen in figure, the equilibrium adsorption capacity of Pb^{2+} raised with the increase of the Pb^{2+} concentration, and the removal rate of Pb^{2+} tended to be stable. When the initial Pb^{2+} concentration was low, the active sites on the TNs surface were not fully utilized and then resulted in lower removal rate. Furthermore, the active site on a certain amount of TNs surface was limited. Consequently, the excess Pb^{2+} were not adsorbed and the Pb^{2+} removal rate reduced because the adsorption sites on the surface of the TNs were utilized when initial Pb^{2+} concentration increased to a certain extent.

When the initial concentration of Pb^{2+} was below 50 mg/L, adsorption capacity increased with time lapse and the removal rate of Pb^{2+} on flaky and linear TNs could be more than 90% (Figs. 6 and 7). The adsorption capacity did not tend to be stable until the initial Pb^{2+} concentration increased to about 200 mg/L. The adsorption capacities of flaky TNs-100, TNs-130, TNs-12, TNs-24, and TNs-36 to Pb^{2+} were determined to be 252.40, 399.00, 479.40, 504.12, and 482.00 mg/g, respectively. Therein, the adsorption capacities of Pb^{2+} on TNs-130 and TNs-24 were the highest. Besides, the adsorption capacities of linear TNs-150, TNs-180, TNs-60, and TNs-72 to Pb^{2+} were up to 311.94, 287.10, 366.60, and 399.00 mg/g, respectively. The results indicated that flaky TNs had higher adsorption capacity and removal effect on Pb^{2+} than the linear TNs. Huang et al. [51] found that the structure of titanate nanoflowers had greater specific surface area and adsorption properties compared with nanotubes and nanowires. Likewise, the results of this experiment were similar.

To further analyze the adsorption behavior of Pb^{2+} on flaky TNs, following experiments would focus on the adsorption of Pb^{2+} by TNs-24 as adsorbent.

3.2.2. Effect of adsorption time

In order to compare the effect of adsorption time on the adsorption properties of TNs, the effect of adsorption time on the adsorption of 100 mg/L Pb^{2+} onto flaky TNs-24 is displayed in Fig. 8. Apparently, flaky TNs-24 could quickly capture Pb^{2+} from solution, as the adsorption mainly occurred in the first 40 min (especially the initial 5 min). It could be divided into two stages. First, the adsorption rate was fastest and the adsorption capacity of Pb^{2+} increased rapidly with time during the first 40 min, especially in the first 5 min. The adsorption capacity of TNs-24 at the first 5 and 40 min was as high as 165.75 and 404.93 mg/g, respectively. The rapid adsorption of this initial adsorption was owing to the presence of a large number of active sites on the surface of the adsorbent [52,53]. Second, the adsorption capacity of Pb^{2+} showed reasonably stable after 40 min. After that, the adsorption reached equilibrium when the reaction time

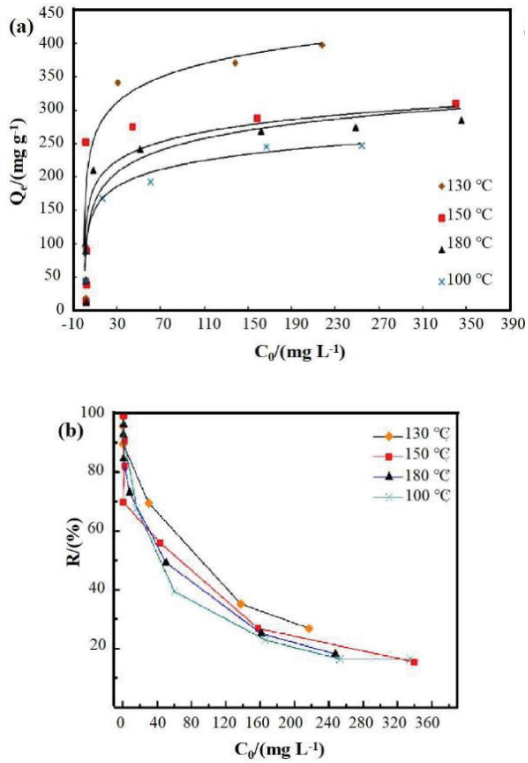

Fig. 6. Removal efficiency of TNs synthesized at different temperatures: (a) TNs-100, (b) TNs-130, (c) TNs-150, and (d) TNs-180.

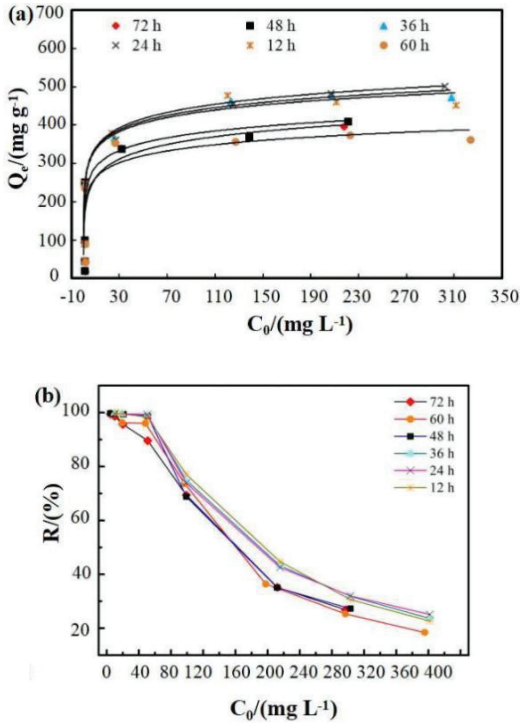

Fig. 7. Removal efficiency of TNs synthesized at different times: (a) TNs-12, (b) TNs-24, (c) TNs-36, (d) TNs-48, (e) TNs-60, and (f) TNs-72.

was 120 min. It was because the adsorption site was continuously consumed with the increased of adsorption time. Afterwards, the adsorption of Pb^{2+} on the material tended to be saturated.

3.2.3. Effect of adsorption temperature

The effect of temperature on the adsorption of Pb^{2+} on flaky TNs-24 is presented in Fig. 9. The equilibrium adsorption capacity under the temperature of 20°C, 40°C, and 60°C of flaky TNs on Pb^{2+} were 504.12, 318.00, and 253.00 mg/g, respectively. It could be observed that the equilibrium adsorption capacity of Pb^{2+} and the corresponding saturated adsorption capacity decreased as the temperature rose. It could also be found that the adsorption process of Pb^{2+} was the exothermic process and the increase of temperature was not conducive to the adsorption of Pb(II). Consequently, the room temperature or lower temperature can satisfy the high adsorption capacity for Pb^{2+} with flaky TNs.

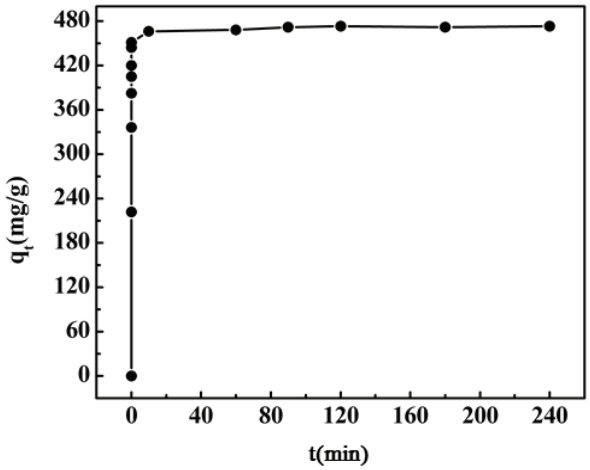

Fig. 8. Effect of contact time on the adsorption of Pb^{2+} by flaky TNs-24.

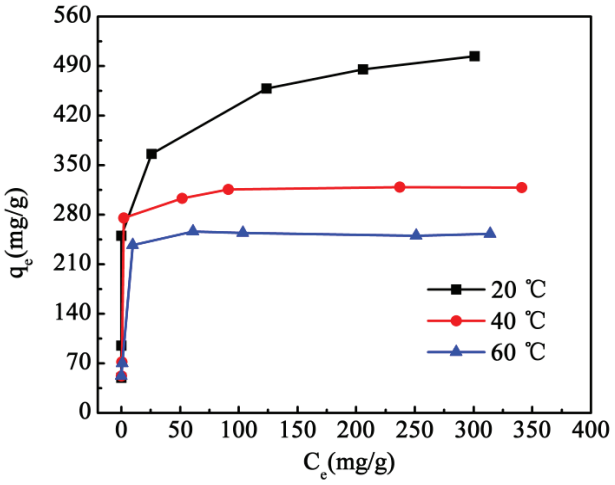

Fig. 9. Effect of temperature on the adsorption of Pb^{2+} by flaky TNs-24.

3.2.4. Effect of pH

Solution pH is one of the most important factors in the adsorption process as it can influence the species of metal ions and the surface charge of the adsorbent [54]. For pH studies, adsorption of Pb^{2+} by flaky TNs-24 was performed over a pH range of 1.0–10.0. The effect of pH on adsorption of Pb^{2+} by flaky TNs-24 and the zeta potential of TNs-24 under different pH are shown in Fig. 10.

From Fig. 10(a), the absorption capacity of Pb^{2+} was obviously influenced by the pH. For Pb^{2+}, when the pH is below 5, the absorption capacity is relatively low. However, with the increase of pH, the absorption capacity increased dramatically. This trend of the curves can be explained by the ionic conditions of functional groups on the TNs. When the pH was less than 5.0, the –OH groups of TNs were protonated and formed a positive surface charge [55], which can also be seen from Fig. 10(b). TNs-24 is positively charged at pH values less than 5. And the competition between the H^+ and Pb^{2+} ions led to a low adsorption capability [56]. The electrostatic repulsion between protonated groups and metal cations as well as the competition of protonated groups with Pb^{2+} for active binding site will result in the decrease of absorption capacity. As the pH increases, the surface of TNs-24 was negatively charged (Fig. 10(b)), hence adsorption could be driven by electrostatic attraction between positively charged adsorbate species (Pb^{2+}) and negative adsorbents. Furthermore, the competition of H^+ ions for active sites decreases with increasing pH [57]. Besides, the total positive charge on the surface of the functional group

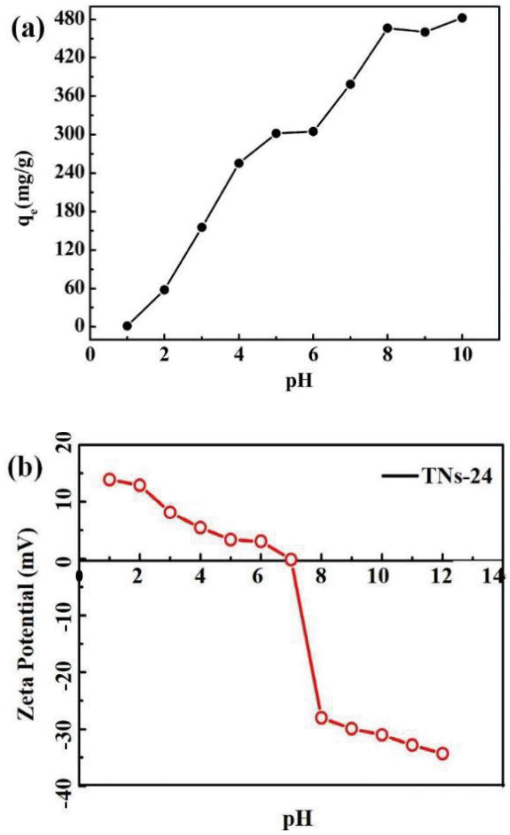

Fig. 10. (a) Effect of pH on adsorption of Pb^{2+} by flaky TNs and (b) zeta potential of TNs-24 in deionized water with different pH.

decreases. Therefore, the degree of protonation is weakened, which is beneficial to the adsorption of Pb(II).

Furthermore, pH can also affect the hydrolysis and precipitation processes as well as the distribution of metal cation species, which will chemically affect the interaction between the metal cation and the adsorbent. Xin et al. [58] show the dominant species of Pb^{2+} in the 100 mg/L aqueous solution calculated by MINTEQ computer code. The dominant species of Pb^{2+} under the investigated pH range (pH 2–7) changed gradually. The dominant species are Pb^{2+} and $PbNO^{3+}$, respectively. Therefore, it can be concluded that the adsorption of Pb^{2+} is not only influenced by the electrostatic interaction, but also affected by the chemisorption process. When the pH was above 5.0, as the pH continued increasing, it was also disadvantageous for adsorbing Pb^{2+} due to the fact that metal hydroxide precipitation may occur in alkaline solution [59]. Therefore, in order to avoid the generation of hydroxide precipitation to the adsorption process caused by interference, the optimum adsorption pH of Pb^{2+} from flaky TNs-24 could be controlled in the range of 5.0–6.0. Others also reported that the adsorption capacity of TNTs to Pb^{2+} was the highest at pH = 5.0, and the adsorption capacity of TNTs to Pb^{2+} was relatively high when pH was in the range of 5.0–6.0 [60]. Herein, 5.0 can be selected as optimum pH for Pb^{2+} adsorption in the following experiments.

3.2.5. Effect of titanate dosage

To find the best titanate dosage for adsorbing of Pb^{2+} in aqueous solutions, the effects of different dosage of TNs-24 were investigated at an initial Pb^{2+} concentration of 100 mg/L. It is shown in Fig. 11. The results indicated that the equilibrium adsorption capacity of TNs-24 to Pb^{2+} was decreasing and removal rate increased rapidly and then became stable with the increasing of TNs-24 dosage. The best dosage of TNs-24 for attaining the maximum adsorption of Pb^{2+} was 0.05 g/L, where the equilibrium adsorption capacity reached 348.60 mg/g and the removal rate reached to the minimum (18.32%) after 120 min of adsorption. When the dosage increased to 1.0 g/L, the equilibrium adsorption capacity reached 94.93 mg/g and the removal rate reached 99.91%. Moreover, the equilibrium adsorption capacity was decreasing, and removal rate was basically unchanged at 99% when the dosing amount was in the range of 0.4–1.0 g/L.

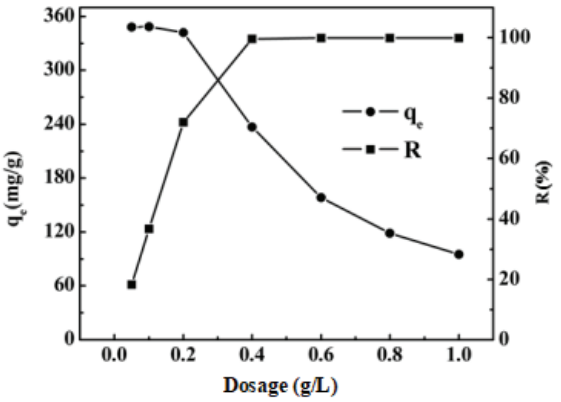

Fig. 11. Effect of adsorbent dosage on adsorption of Pb^{2+} by flaky TNs.

The effect of the amount of adsorbent on the adsorption effect is mainly related to the specific surface area of the adsorbent and the number of adsorption sites [61].The saturated adsorption with higher adsorption capacity could be attributed to the limited surface area and adsorption sites when the amount of flaky TNs was less. Therefore, the removal rate was low due to the limited adsorption sites were not enough to adsorb a large amount of Pb(II). After that, the Pb^{2+} content decreased with the increase of dosing amount. It could account for the adsorption site of TNs appeared excess and could not be fully utilized when the specific surface area and the number of adsorption sites increased.

3.2.6. Competitive adsorption experiment

Actual wastewater usually contains a variety of metal ions. Therefore, the selective adsorption of different metal ions onto TNs is very important for its further practical use. Herein, the adsorption behavior of Pb^{2+}, Cd^{2+}, and Ni^{2+} onto TNs was studied.

The effect of different concentrations of Cd^{2+} or Ni^{2+} on the adsorption of Pb^{2+} by TNs-24 is shown in Fig. 12. Results showed that the presence of Cd^{2+} or Ni^{2+} does not affect Pb^{2+} adsorption significantly. When the initial concentration of Cd^{2+} was 25 mg/L, the equilibrium adsorption and removal

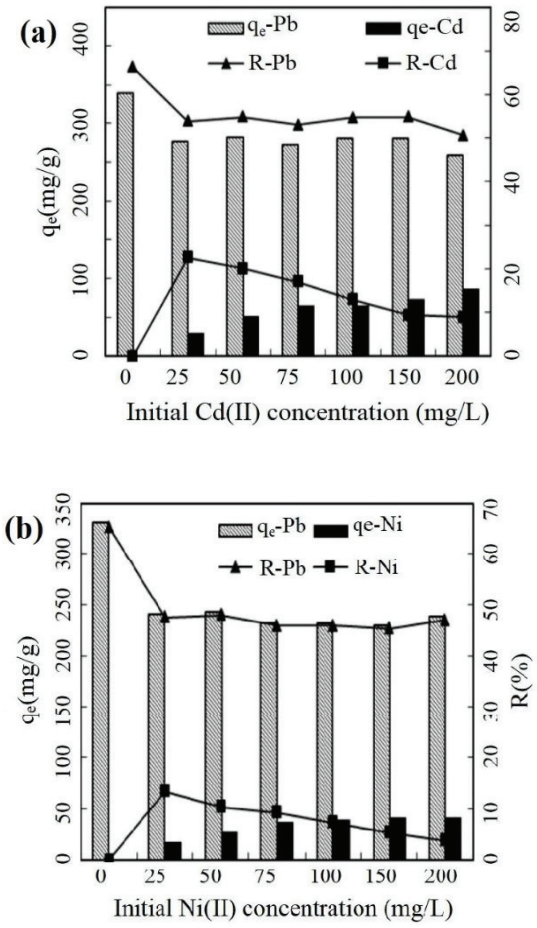

Fig. 12. Effect of various coexistent heavy metal ions on adsorption of Pb^{2+} by TNs-24.

rate of Pb^{2+} decreased to 62.90 mg/g and 12.24%, respectively. However, as the initial concentration of Cd^{2+} continued to increase (25–200 mg/L), the equilibrium adsorption capacity and removal rate of TNs-24 to Pb^{2+} changed little. In addition, as the initial concentration of Cd^{2+} continues to increase, the equilibrium adsorption capacity of Cd^{2+} on TNs-24 slightly increased. This small decrease in adsorption capacity could be due to the competition for adsorption sites of Pb^{2+} at lower Cd^{2+} concentration [62]. Moreover, the presence of Ni^{2+} also led to a decrease in Pb^{2+} adsorption capacity, and this effect was more significant for the presence of Ni^{2+} as shown in Fig. 12(b).

Obviously, Pb^{2+} still has a removal rate of more than 50%, revealing that TNs-24 is still a good adsorbent for removing Pb^{2+}. As we know, Pb^{2+} is one of the most toxic elements. The highest efficiency for Pb^{2+} removal by TNs-24 is thus tremendously important for the environmental protection and the cost saving of purification operations.

3.2.7. Regeneration of the adsorbent

Regeneration of the adsorbent material is of great importance in economic development, because it helps to protect the environment through recycling of the adsorbate and adsorbent [42]. Desorption studies were conducted to determine the feasibility of regenerating the flaky titanate adsorbent using HCl as eluent. Desorption rates of Pb(s) from flaky TNs-24 via different pH are presented in Fig. 13. It was found that when the pH is 1.0, the desorption rate of TNs-24 can reach 99.00%. When the pH of the solution is in the range of 1.0–3.0, the desorption rate of the material decreases as the pH increases. While the pH is in the range of 4.0–6.0, Pb^{2+} can hardly be desorbed and the desorption rate is zero. The results show that HCl has a good desorption effect on Pb^{2+}. After six cycles of adsorption—desorption experiments, the Pb^{2+} removal efficiency of the flaky titanate adsorbent was still above 90%, showing characteristics of a good adsorbent (Table 2).

3.3. Adsorption mechanism of flaky TNs to Pb^{2+}

3.3.1. Modeling of the adsorption kinetics

To further analyze the adsorption mechanism of Pb^{2+} adsorbed by flaky TNs, the adsorption kinetics of Pb^{2+} adsorbed by TNs was studied. The adsorption data of Pb^{2+} were analyzed by three kinetic models: pseudo-first-order kinetic model, pseudo-second-order kinetics model, and Weber particle diffusion model (the related formulas are shown in Table 3).

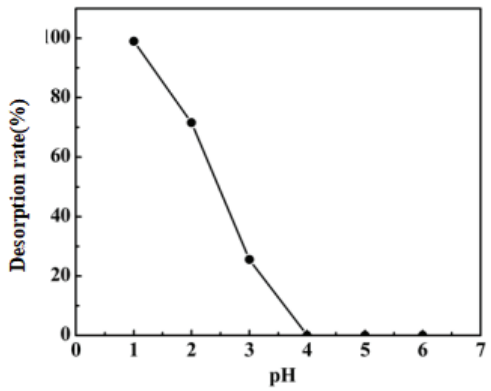

Fig. 13. Effect of pH on desorption of Pb^{2+} by TNs-24.

Simulated parameters for adsorption kinetics are given in Table 4. It could be found that the adsorption of Pb^{2+} onto flaky TNs could be well described by pseudo-second-order kinetic model (R^2 = 0.9986). Furthermore, the pseudo-second-order model had the lowest SSE value (0.0532) relative to SSE = 0.118 for the pseudo-first-order model, and hence the second-order model can be used to describe the adsorption of Pb^{2+} onto flaky TNs. Moreover, lower R^2 values for Weber particle diffusion model suggested it cannot be used to describe the adsorption of Pb^{2+} onto flaky TNs. While little deviations between experimental date (487.62 mg/g) and calculated adsorption capacity (481.00 mg/g) were found, chemical adsorption was the rate-controlling step in the adsorption process [63].

3.3.2. Modeling of adsorption isotherm

The adsorption isotherm can reflect the distribution of adsorbate in the adsorbent and solution and the adsorption capacity of the adsorbent to the adsorbate. To obtain insight into the possible mechanisms for removing Pb^{2+} ions from aqueous solution onto flaky TNs, the adsorption equilibrium data were analyzed using Langmuir, Freundlich, and Temkin models (Table 5).

Fig. 14 depicts the adsorption isotherms of Pb^{2+} onto TNs-24. It could be seen that the equilibrium adsorption data were fitted well with Langmuir model, followed by Temkin model, and the Freundlich model had the worst fitting effect. The corresponding parameters are listed in Table 6. Overall, the Langmuir isotherm model correlation coefficient was significantly closer to unity (R^2 = 0.9958) relative to that of the Temkin model (R^2 = 0.94705) and the Freundlich isotherm model (R^2 = 0.88189). Moreover, the chi-square value for the Langmuir isotherm model (χ^2 = 1.345) is lower than that of the Temkin model ((χ^2 = 11.054) and the Freundlich isotherm model ((χ^2 = 21.042) further indicating that the experimental data fit the Langmuir isotherm model better. The Langmuir

Table 2
The recycled adsorption of Pb^{2+} by TNs-des and TNs-re

Metal	Adsorbent	Cycles	q_e (mg/g)	R (%)	D (%)
Pb^{2+}	TNs-des	1*	170.47	99.98	93.22
		2	141.81	83.17	96.91
		3	59.25	30.48	94.30
		4	31.75	16.33	99.21
		5	10.13	5.57	91.36
		6	8.63	4.74	92.46
	TNs-re	1*	170.47	99.98	98.83
		2	173.98	99.06	97.95
		3	171.73	99.99	98.11
		4	171.71	99.98	98.84
		5	169.13	98.47	99.56
		6	166.74	97.08	96.56

*The adsorbents used for the first cycles were all newly prepared TNs-24.

Table 3
Modeling of the adsorption kinetics

Kinetic model	Formula	Kinetic parameters
Pseudo-first-order kinetic model	$\log(q_e - q_t) = \log q_e - \frac{k_1}{2.303}$	q_e and q_t are the adsorption capacity (mg/g) of the material for Pb^{2+} at equilibrium time and at time t; t is the adsorption time (min); k_1 is the pseudo-first-order kinetic rate constant (min^{-1})
Pseudo-second-order kinetic model [63]	$\frac{t}{q_t} = \frac{1}{k_2 q_e^2} + \frac{1}{q_e}$	k_2 is the pseudo-first-order kinetic rate constant (g/(mg·min))
Intraparticle diffusion model [64]	$q_t = k_{int} t^{0.5} + C$	k_{int} is the intraparticle diffusion rate constant (mg/(g·$min^{0.5}$)); C is the constant (mg/g) associated with the thickness of the boundary layer

Table 4
Kinetic parameters of adsorption of Pb^{2+} by TNs-24

Kinetic model	Kinetic parameters	Pb^{2+}
Pseudo-first-order kinetics model	q_e (mg/g)	454.3
	k_1 (1/min)	479.19
	R^2	0.96412
	SSE	0.118
Pseudo-second-order kinetics model	q_e (mg/g)	487.62
	k_2 (g/(mg·min))	1.87
	R^2	0.9986
	SSE	0.0532
Weber particle diffusion model	k_{int} (mg/(g·$min^{0.5}$))	11.14
	C (mg/g)	343.2
	R^2	0.1699
	SSE	3.044

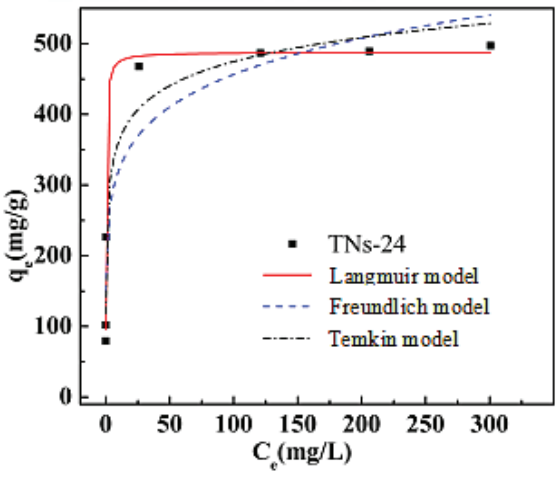

Fig. 14. Adsorption isotherm for the adsorption of Pb^{2+} by TNs-24.

Table 5
Modeling of adsorption isotherm

Isotherm model	Formula	Kinetic parameters
Langmuir	$\frac{C_e}{q_e} = \frac{1}{bQ} - \frac{1}{Q} C_e$	q_e is the equilibrium adsorption capacity (mg/g) of Pb (II); C_e is the equilibrium concentration (mg/L) of Pb (II); Q is the saturated adsorption capacity (mg/g) of Pb (II); b is Langmuir constant, its size is related to the adsorption free energy (L/g)
Freundlich	$\log q_e = \log K_F - \frac{1}{n} \log C_e$	K_F is the Freundlich constant, which is related to the adsorption capacity of heavy metal ions (mg/g); n is the nonuniform factor, which represents the adsorption intensity of heavy metal ions
Temkin	$q_e = \frac{RT}{B} \ln A - \frac{RT}{B} \ln C_e$	A (L/g) and B (J/mol) are both Temkin constants, R (J/mol K) is the ideal gas constant, and T (K) is the absolute temperature

model supposed there were monolayer adsorption sites on the adsorbent's surface and no interaction between adsorbates. In addition, the calculated adsorption capacity (587.86 mg/g) of flaky TNs-24 to Pb^{2+} was close to that obtained by the experiment.

3.3.3. Comparison of flaky TNs with other adsorbents

The comparison of the maximum adsorption capacities of Pb^{2+} ions onto different adsorbents is presented in Table 7. The flaky titanate adsorbents under study have a reasonable and competitive adsorption capacity as compared with other adsorbents, making it a potential adsorbent for removal of Pb^{2+} ions from aqueous solutions.

3.3.4. Adsorption mechanism of flaky TNs to Pb^{2+}

In summary, the adsorption of heavy metals by flaky TNs could be attributed to the interaction of heavy metal ions with hydroxyl groups in TNs. The mechanism of adsorption

Table 6
Isotherm parameters of adsorption of Pb^{2+} by TNs-24

Isotherm model	Kinetic parameters	Pb^{2+}
Langmuir	Q (mg/g)	487.86
	b (L/mg)	3.49
	R^2	0.99518
	χ^2	1.345
Freundlich	K_F (mg/g)	225.31
	n	6.52
	R^2	0.88189
	χ^2	21.042
Temkin	A (L/g)	158.4
	B (J/mol)	50.49
	R^2	0.94705
	χ^2	11.054

Table 7
Comparison of flaky TNs with other adsorbents

Adsorbent	Metal	pH	Adsorbent capacity (mg/g)	Reference
CNC composite with bentonite	Pb^{2+}	5	91.2	[65]
NFC composite with CMC	Pb^{2+}	5	74.8	[66]
CF/poly(NIPAM-co-AAc)	Pb^{2+}	6	80.8	[67]
Titanate nanofiber	Pb^{2+}	6–7	279.72	[68]
Titanate nanoflower	Pb^{2+}	–	147.52	[51]
Titanate nanowire	Pb^{2+}	–	399.005	This work
Titanate nanosheet	Pb^{2+}	5	504.12	This work

CNC — Cellulose nano-crystals; NFC — nanofibrillated cellulose; CMC — carboxymethylcellulose; CF/poly(NIPAM-co-AAc) — cellulose filament as the reinforcement scaffold and crosslinked copolymer of, N-isopropylacrylamide as the thermosensitive component and acrylic acid.

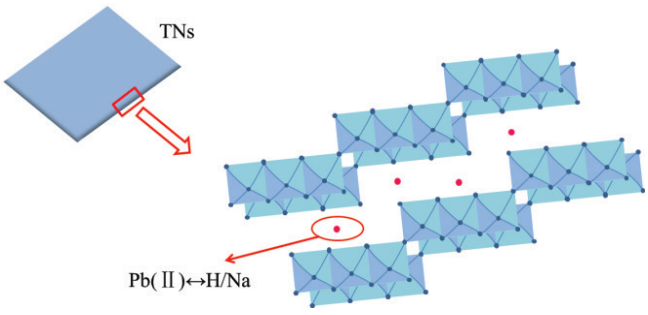

Fig. 15. Schematic of Pb^{2+} adsorption onto flaky TNs.

of Pb^{2+} by flaky TNs is shown in Fig. 15, which clarifies the lamellar structure of flaky TNs and the adsorption process of Pb^{2+} onto TNs. In the experiment, the pH of the solution was 5.18, which was larger than the zero potential (2.57–4.3) of TNs. Consequently, the positively charged Pb^{2+} could easily contact with flaky TNs surface due to electrostatic interaction between positively charged metal cations and the negatively charged surface. Thus, Pb^{2+} had ion exchange with H^+ and Na^+ on the surface of the flaky TNs during the adsorption process [61].

4. Conclusions

In conclusion, flaky TNs had higher adsorption and removal effects on Pb^{2+} than linear TNs. The adsorption mechanism of flaky TNs to Pb^{2+} was mainly due to the ion exchange between Pb^{2+} and hydroxyl as well as H^+/Na^+ in flaky TNs. Compared with the linear TNs, the flaky TNs had a strong absorption capacity. Besides, the reaction temperature or reaction time had a certain impact on the TNs morphology and adsorption properties. Comparing with the linear structure, the flaky TNs exhibited larger adsorption capacity and faster kinetics. The reaction temperature and reaction time of the prepared TNs with high adsorption capability were 130°C and 12–24 h, respectively. The adsorption kinetics of Pb^{2+} followed pseudo-second-order model, and the equilibrium data fitted well with Langmuir model. Overall, flaky TNs showed excellent adsorptive for the removal of Pb^{2+} from wastewater and could be employed as a low-cost alternative adsorbent.

Acknowledgments

The authors would like to gratefully acknowledge the financial support from the National Natural Science Foundation of China (no. 51778146), the Outstanding Youth Fund of Fujian Province in China (no. 2018J06013), the China Postdoctoral Science Foundation (no. 2014M561856), and the open test fund for valuable instruments and equipment of Fuzhou University (no. 2018T033).

References

[1] F.N. Muya, C.E. Sunday, P.P.U.A. Baker, E. Iwuoha, Environmental remediation of heavy metal ions from aqueous solution through hydrogel adsorption: a critical review, Water Sci. Technol., 73 (2016) 983–992.
[2] C.M. Monteiro, P.M.L. Castro, F.X. Malcata, Biosorption of zinc ions from aqueous solution by the microalga *Scenedesmus obliquus*, Environ. Chem. Lett., 9 (2011) 169–176.
[3] M. Min, L. Shen, G. Hong, M. Zhu, Y. Zhang, X.W.D.E. Wang, Y.Y.D.E. Chen, B.S. Hsiao, Micro-nano structure poly(ether sulfones)/poly(ethyleneimine) nanofibrous affinity membranes for adsorption of anionic dyes and heavy metal ions in aqueous solution, Chem. Eng. J., 197 (2012) 88–100.
[4] Y.X. Liu, X. Wu, D. Yuan, J. Yan, Removal of nickel from aqueous solution using cathodic deposition of nickel hydroxide at a modified electrode, J. Chem. Technol. Biotechnol., 88 (2013) 2193–2200.
[5] D. Chen, T. Awut, B. Liu, Y. Ma, T. Wang, I. Nurulla, Functionalized magnetic Fe_3O_4 nanoparticles for removal of heavy metal ions from aqueous solutions, e-Polymers, 16 (2016) 313–322.
[6] M. Zhao, Y. Xu, C.G.G.E. Zhang, H. Rong, G. Zeng, New trends in removing heavy metals from wastewater, Appl. Microbiol. Biotechnol., 100 (2016) 6509–6518.
[7] R.D.R.R. Dhankhar, A. Hooda, Fungal biosorption – an alternative to meet the challenges of heavy metal pollution in aqueous solutions, Environ. Technol., 32 (2011) 467–491.
[8] H. Qi, X. Jiang, D. Zhou, B. Zhu, L. Qin, C. Ma, Y. Ong, Y. Murata, Removal of heavy metals in aqueous solution using

Antarctic krill chitosan/hydroxyapatite composite, Fibers Polym.,14 (2013) 1134–1140.
[9] K. He, Y. Chen, Z. Tang, Y. Hu, Removal of heavy metal ions from aqueous solution by zeolite synthesized from fly ash, Environ. Sci. Pollut Res., 23 (2016) 2778–2788.
[10] R. Kishor, A.K. Ghoshal, APTES grafted ordered mesoporous silica KIT-6 for CO_2 adsorption, Chem. Eng. J., 262 (2015) 882–890.
[11] K.G.S. SenGupta, Adsorption of a few heavy metals on natural and modified kaolinite and montmorillonite: a review, Adv. Colloid Interface Sci., 140 (2008) 114–131.
[12] R.A. Doong, C.Y. Liao, Enhanced visible-light-responsive photodegradation of bisphenol A by Cu, N-codoped titanate nanotubes prepared by microwave-assisted hydrothermal method, J. Hazard. Mater., 32 (2017) 254–262.
[13] A.J.M.B. Junqian Ding, and A.M.Y.A. Chunhe Li, Study of the enhanced visible-light-sensitive photocatalytic activity of Cr_2O_3-loaded titanate nanosheets for Cr(VI) degradation and H_2 generation, Catal. Sci. Technol., 7 (2017) 2283–2297.
[14] M.R. Morris, S.R. Pendlebury, J. Hong, S. Dunn, J.R. Durrant, Effect of internal electric fields on charge carrier dynamics in a ferroelectric material for solar energy conversion, Adv. Mater., 28 (2016) 7123–7128.
[15] P. Meenakshi, M. Selvaraj, Bismuth titanate as an infrared reflective pigment for cool roof coating, Sol. Energy Mater. Sol. Cells, 174 (2018) 530–537.
[16] Q. Tian, Impressive lithium storage properties of layered sodium titanate with hierarchical nanostructures as anode materials for lithium-ion batteries, J. Alloys Compd., 699 (2017) 540–547.
[17] Y. Hui, L. Cao, Z. Xu, J.H.C. Huang, H. Ouyang, J. Li, Synthesis of $Li_4Ti_5O_{12}$ nanoclusters for lithium-ion batteries with excellent electrochemical performances, J. Electroanal. Chem., 763 (2016) 32–36.
[18] E. Song, Y. Chen, A. Li, Y. Sun, R. Yang, J. Wang, H. Zhang, J. Li, D. Zhang, Preparation and adsorbing performance of calcium titanate with template method, Mater. Manuf. Processes, 32 (2017) 1428–1434.
[19] G. Fan, R. Lin, Z. Su, X. Lin, R.X.A.W. Chen, Removal of Cr (VI) from aqueous solutions by titanate nanomaterials synthesized via hydrothermal method, Can. J. Chem. Eng., 95 (2017) 717–723.
[20] J. Huang, Y. Cao, Z. Liu, Z. Deng, W. Wang, Application of titanate nanoflowers for dye removal: a comparative study with titanate nanotubes and nanowires, Chem. Eng. J., 191 (2012) 38–44.
[21] M.A.A.L.T. Mohammadi, Adsorption of divalent heavy metal ions from water using carbon nanotube sheets, J. Hazard. Mater., 185 (2011) 140–147.
[22] Q. Chen, L.M. Peng, Structure and applications of titanate and related nanostructures, J. Hazard. Mater., 4 (2007) 44–65.
[23] B. Filipowicz, M. Pruszyński, S. Krajewski, A. Bilewicz, Adsorption of 137Cs on titanate nanostructures, J. Radioanal. Nucl. Chem., 301 (2014) 889–895.
[24] L. Xiong, C. Chen, Q.C.A.J. Ni, Adsorption of Pb^{2+} and Cd^{2+} from aqueous solutions using titanate nanotubes prepared via hydrothermal method, J Hazard. Mater., 189 (2011) 741–748.
[25] N. Li, L. Zhang, Y. Chen, Y.T.A.H. Wang, Adsorption behavior of Cu^{2+} onto titanate nanofibers prepared by alkali treatment, J. Hazard. Mater., 189 (2011) 265–272.
[26] H.H.K.Y. Kochkar, Study of Pd^{2+} adsorption over titanate nanotubes of different diameters, J. Colloid Interface Sci., 331 (2009) 27–31.
[27] C. Shi, H. He, Z. Hong, H. Zhan, M. Feng, Effect of HCl post-treatment on morphology of hydrothermally prepared titanate nanomaterials with optical limiting properties, Acta Phys. Chim. Sin., 31 (2015) 1430–1436.
[28] L. Xiong, C. Chen, Q.C.A.J. Ni, Adsorption of Pb(II) and Cd(II) from aqueous solutions using titanate nanotubes prepared via hydrothermal method, J. Hazard. Mater., 89 (2011) 741–748.
[29] J. Chen, M.C. Che, F. Yan, Synthesis of barium strontium titanate nanopowders by microwave hydrothermal method, Adv. Appl. Ceram., 114 (2015) 344–349.
[30] L. Persano, A. Camposeo, C. Tekmen, D. Pisignano, Industrial upscaling of electrospinning and applications of polymer nanofibers: a review, Macromol. Mater. Eng., 298 (2013) 504–520.
[31] S. Haider, S. Park, Preparation of the electrospun chitosan nanofibers and their applications to the adsorption of Cu^{2+} and Pb^{2+} ions from an aqueous solution, J. Membr. Sci., 328 (2009) 90–96.
[32] M.I. Shariful, S.B. Sharif, J.J.L. Lee, U. Habiba, B.C. Ang, M.A. Amalina, Adsorption of divalent heavy metal ion by mesoporous-high surface area chitosan/poly (ethylene oxide) nanofibrous membrane, Carbohydr. Polym., 157 (2017) 57–64.
[33] M.K.E.W. Miyazaki, Protonated titanate nanotubes with lewis and brønsted acidity: relationship between nanotube structure and catalytic activity, Chem. Mater., 25 (2013) 385–393.
[34] J. Nian, H. Teng, Hydrothermal synthesis of single-crystalline anatase TiO_2 nanorods with nanotubes as the precursor, J. Phys. Chem. B, 110 (2006) 4193–4198.
[35] X. Nie, Y. Teh, Titanate nanotubes as superior adsorbents for removal of lead^{2+} ions from water, Mater. Chem. Phys., 123 (2010) 494–497.
[36] Y. Chen, S.S.N.E. Lo, J. Kuo, Pb^{2+} adsorption capacity and behavior of titanate nanotubes made by microwave hydrothermal method, Colloids Surf., A, 361 (2010) 126–131.
[37] M. Huang, S. Li, X.G. Li, Longan shell as novel biomacromolecular sorbent for highly selective removal of lead and mercury ions, J. Phys. Chem. B, 114 (2010) 3534–3542.
[38] L.Y. Wang, L.Q. Yang, Y.F. Li, Y. Zhang, X.J. Ma, Z. F. Ye, Study on adsorption mechanism of Pb^{2+} and Cu^{2+} in aqueous solution using PS-EDTA resin, Chem. Eng. J., 163 (2010) 364–372.
[39] H. Nadaroglu, E.E.A.E. Kalkan, N. Demir, Removal of copper from aqueous solution using red mud, Desalination, 251 (2010) 90–95.
[40] S.T.A. Kurniawan, Low-cost adsorbents for heavy metals uptake from contaminated water: a review, J. Hazard. Mater., 97 (2003) 219–243.
[41] U. Guyo, Application of response surface methodology for Cd^{2+} adsorption on maize tassel-magnetite nanohybrid adsorbent, J. Environ. Chem. Eng., 3 (2015) 2472–2483.
[42] U.G.K.S. Moyo, Removal of nickel^{2+} from aqueous solution by Vigna unguiculata (cowpea) pods biomass, Water Sci. Technol., 73 (2016) 2301–2310.
[43] W. Liu, A.G.L. Borthwick, X. Li, J. Ni, High photocatalytic and adsorptive performance of anatase-covered titanate nanotubes prepared by wet chemical reaction, Microporous Mesoporous Mater., 186 (2014) 168–175.
[44] J. Huang, Y. Cao, Z.D.A.H. Tong, Formation of titanate nanostructures under different NaOH concentration and their application in wastewater treatment, J. Solid State Chem., 184 (2011) 712–719.
[45] B. Buchholcz, E. Varga, T. Varga, K. Plank, J. Kiss, Z. Kónya, Structure and stability of boron doped titanate nanotubes and nanowires, Vacuum, 138 (2017) 120–124.
[46] V. Bem, M.C. Neves, M.R. Nunes, A.J. Silvestre, O.C. Monteiro, Influence of the sodium/proton replacement on the structural, morphological and photocatalytic properties of titanate nanotubes, Condens. Matter Phys., 232 (2012) 50–56.
[47] H.L.R.L. Dana L. Morgan, Implications of precursor chemistry on the alkaline hydrothermal synthesis of titania/titanate nanostructures, J. Phys. Chem. C, 114 (2010) 101–110.
[48] W. Liu, X. Zhao, T. Wang, D.Z.A.E. Zhao, J.N.I.P. Ni, Adsorption of U(VI) by multilayer titanate nanotubes: effects of inorganic cations, carbonate and natural organic matter, Chem. Eng. J., 286 (2016) 427–435.
[49] T. Wang, W. Liu, N. Xu, J. Ni, Adsorption and desorption of Cd^{2+} onto titanate nanotubes and efficient regeneration of tubular structures, J. Hazard. Mater., 250–251 (2013) 379–386.
[50] J. Huang, Y. Cao, Q. Huang, H. He, Y. Liu, W. Guo, M. Hong, High-temperature formation of titanate nanotubes and the transformation mechanism of nanotubes into nanowires, Cryst. Growth Des., 9 (2009) 3632–3637.
[51] J. Huang, Y. Cao, Z. Liu, Z. Deng, F. Tang, W. Wang, Efficient removal of heavy metal ions from water system by titanate nanoflowers, Chem. Eng. J., 180 (2012) 75–80.

[52] M.M.R.Y. Rafatullah, O. Sulaiman, R. Hashim, A. Ahmad, Adsorption of copper (II), chromium (III), nickel $^{2+}$ and lead $^{2+}$ ions from aqueous solutions by meranti sawdust, Chem. Eng. J., 170 (2009) 969–977.
[53] S.E.A. Sharaf El-Deen, N.S. Ammar, T.S. Jamil, Adsorption behavior of Co^{2+} and Ni^{2+} from aqueous solutions onto titanate nanotubes, Fullerenes Nanotubes Carbon Nanostruct., 24 (2016) 455–466.
[54] P. Gu, J. Xing, T. Wen, R. Zhang, J. Wang, G. Zhao, T. Hayat, Y. Ai, Z. Lin, X. Wang, Experimental and theoretical calculation investigation on efficient Pb^{2+} adsorption on etched Ti_3AlC_2 nanofibers and nanosheets, Environ. Sci. Nano., 5 (2018) 946–955.
[55] H. Xin, Y. Jinyue, W. Jingkang, B. Jingtao, X. Chuang, H. Hongxun, Design and synthesis of core–shell Fe_3O_4@PTMT composite magnetic microspheres for adsorption of heavy metals from high salinity wastewater, Chemosphere, 206 (2018) 513–521.
[56] J. Wang, Q. Yang, L. Zhang, M. Liu, N. Hu, W. Zhang, W. Zhu, R. Wang, Y. Suo, J. Wang, A hybrid monolithic column based on layered double hydroxide-alginate hydrogel for selective solid phase extraction of lead ions in food and water samples, Food Chem., 257 (2018) 155–162.
[57] Z. Min, L. Yuan, Y. Qili, H. Liulian, C. Lihui, N. Yonghao, X. Huining, Temperature and pH responsive cellulose filament/poly(NIPAM-co-AAc) hybrids as novel adsorbent towards Pb^{2+} removal, Carbohydr. Polym., 195 (2018) 495–504.
[58] H. Xin, Y. Jinyue, W. Jingkang, B. Jingtao, X. Chuang, H. Hongxun, Design and synthesis of core-shell Fe3O4@PTMT composite magnetic microspheres for adsorption of heavy metals from high salinity wastewater, Chemosphere, 206 (2018) 513–521.
[59] S. Ma, J. Zhang, D. Sun, G. Liu, Surface complexation modeling calculation of Pb^{2+} adsorption onto the calcined diatomite, Appl. Surf. Sci., 359 (2015) 48–54.
[60] W. Liu, T. Wang, A.G.L. Borthwick, Y. Wang, X. Yin, X. Li, J. Ni, Adsorption of Pb^{2+}, Cd^{2+}, Cu^{2+} and Cr^{3+} onto titanate nanotubes: competition and effect of inorganic ions, Sci. Total Environ., 456–457 (2013) 171–180.
[61] W. Liu, P. Zhang, A.G.L. Borthwick, H. Chen, J. Ni, Adsorption mechanisms of thallium(I) and thallium(III) by titanate nanotubes: ion-exchange and co-precipitation, J. Colloid Interface Sci., 423 (2014) 67–75.
[62] N. Abdehagh, F. Tezel, J. Thibault, Adsorbent screening for biobutanol separation by adsorption: kinetics, isotherms and competitive effect of other compounds, Adsorption, 19 (2013) 1263–1272.
[63] Y.S.H.A. McKay, Sorption of dye from aqueous solution by peat, Chem. Eng. J., 70 (1998) 115–124.
[64] W.J. Weber, J.C. Morris, Kinetics of adsorption carbon from solutions, J. Sanit. Eng. Div. Proc., ASCE, 89 (1963) 31–60.
[65] B. Chen, Q. Zheng, J. Zhu, J. Li, Z. Cai, L. Chen, S. Gong, Mechanically strong fully biobased anisotropic cellulose aerogels, RSC Adv., 6 (2016) 96518–96526.
[66] J.N. Putro, S.P. Santoso, S. Ismadji, Y. Ju, Investigation of heavy metal adsorption in binary system by nanocrystalline cellulose–bentonite nanocomposite: improvement on extended Langmuir isotherm model, Microporous Mesoporous Mater., 246 (2017) 166–177.
[67] Z. Min, L. Yuan, Y. Qili, H. Liulian, C. Lihui, N. Yonghao, X. Huining, Temperature and pH responsive cellulose filament/poly (NIPAM-co-AAc) hybrids as novel adsorbent towards Pb^{2+} removal, Carbohydr. Polym., 195 (2018) 495–504.
[68] D. Yang, Z. Zheng, H. Liu, H. Zhu, X. Ke, Y. Xu, D.W.A.Y. Sun, Layered titanate nanofibers as efficient adsorbents for removal of toxic radioactive and heavy metal ions from water, J. Phys. Chem. C, 112 (2008) 16275–16280.